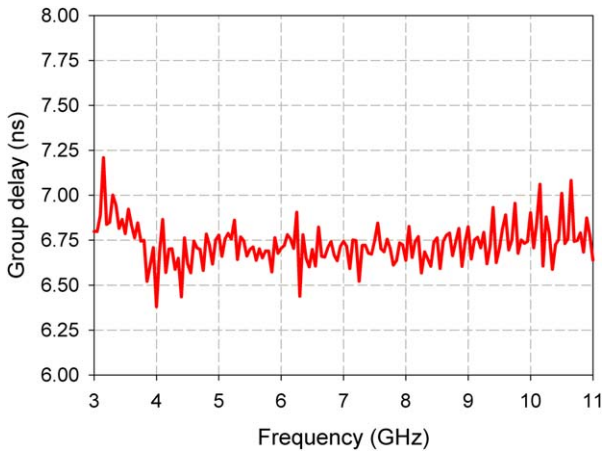

Figure 9 Measured group delay. [Color figure can be viewed in the online issue, which is available at wileyonlinelibrary.com]

The proposed antenna can be useful for UWB communications applications.

REFERENCES

1. H. Schantz, The art and science of ultrawideband antennas, Artech House, Norwood, 2005.
2. L. Jianxin, C.C. Chiau, C. Xiaodong, and C.G. Parini, Study of a printed circular disc monopole antenna for UWB systems, IEEE Trans Antennas Propag 53 (2005), 3550–3554.
3. J. Liu, S. Zhong, and K.P. Esselle, A printed elliptical monopole antenna with modified feeding structure for bandwidth enhancement, IEEE Trans Antennas Propag 59 (2011), 667–670.
4. J. Liu, K.P. Esselle, S.G. Hay, and S. Zhong, Effects of printed UWB antenna miniaturization on pulse fidelity and pattern stability, IEEE Trans Antennas Propag 62 (2014), 3903–3910.
5. K.G. Thomas and M. Sreenivasan, Printed elliptical monopole with shaped ground plane for pattern stability, Electron Lett 45 (2009), 445–446.
6. J. Wang and Y. Yingzeng, Differential-fed UWB microstrip antenna with improved radiation patterns, Electron Lett 50 (2014), 1412–1414.
7. J. Yeo and J.I. Lee, Coupled-sectorial-loop antenna with circular sectors for super wideband applications, Microwave Opt Technol Lett 56 (2014), 1683–1689.
8. J. Yeo and J.I. Lee, Wideband directive folded semicircular dipole antenna, Microwave Opt Technol Lett 56 (2014), 2513–2516.

AN ULTRATHIN PENTA-BAND POLARIZATION-INSENSITIVE COMPACT METAMATERIAL ABSORBER FOR AIRBORNE RADAR APPLICATIONS

Anamiya Bhattacharya, Somak Bhattacharyya, Saptarshi Ghosh, Devkinandan Chaurasiya, and Kumar Vaibhav Srivastava
Department of Electrical Engineering, Indian Institute of Technology, Kanpur, Uttar Pradesh, India; Corresponding author: joysaptarshi@gmail.com

Received 4 April 2015

ABSTRACT: *In this article, an ultrathin penta-band polarization-insensitive metamaterial absorber has been presented, which consists of an array of a closed ring embedded in a tetra-arrow resonator. The proposed ultrathin (~λ_0/18 corresponding to the highest absorption frequency) structure exhibits five distinct absorption peaks at 3.4, 8.34, 9.46, 14.44, and 16.62 GHz with peak absorptivities of 98.6%, 96.6%, 90.1%, 97.8%, and 93.1%, respectively. Due to fourfold symmetry the structure provides nearly unity absorption for all polarization angles under normal incidence. The structure also exhibits high absorption peaks (~80%) up to 45° incident angles for both TE and TM polarizations. Surface current and electric field distributions for different absorption frequencies have been analyzed to visualize the absorption mechanism of the structure. Finally, the structure has been fabricated and experimentally measured responses are in good agreement with the simulated ones.* © 2015 Wiley Periodicals, Inc. Microwave Opt Technol Lett 55:2519–2524, 2015; View this article online at wileyonlinelibrary.com. DOI 10.1002/mop.29365

Key words: *metamaterial; microwave absorber; polarization-insensitivity; penta-band*

1. INTRODUCTION

The unprecedented growth of metamaterial (MTM) [1] in recent years has attracted wide attention due to their unusual electromagnetic properties which leads to ample engineering applications in absorber, imaging, cloaking, and antenna systems [2–7]. The constitutive electromagnetic properties can be manipulated in MTM absorbers such that the input impedance of the structure can be closely matched with the free space impedance, resulting in nearly unity absorptivity [2]. Researches on MTM-based absorbers are very promising nowadays as the thickness can be reduced considerably compared with the conventional absorbers. Several designs of MTM absorbers have been proposed like single-band [8], multiband [9–15], and bandwidth-enhanced structures [16–18].

The aim of this article is to propose a compact ultrathin penta-band polarization-insensitive MTM absorber with wide incident angle, where the absorption peaks are distributed across S, X, and K_u bands. The unit cell of the proposed structure comprises a single ring embedded inside a tetra-arrow resonator. The proposed absorber is polarization-insensitive in design and also provides high absorption (~80%) up to 45° incident angles under oblique incidences. Surface current and electric field distributions have also been studied for investigating the origin of electric and magnetic excitations over the structure. Finally a prototype of the proposed absorber has been fabricated on a 1 mm thick FR4 dielectric substrate and reflection from the structure has been measured in anechoic chamber. Both the numerical simulation and experimental measurements ensure that the proposed absorber provides penta-band absorption peaks along with polarization-insensitivity and wide-angle characteristics.

2. DESIGN OF THE STRUCTURE AND SIMULATION RESULTS

The top view of the unit cell of the proposed penta-band structure has been shown in Figure 1(a). The directions of the incident electric field, magnetic field and wave propagation vectors are also shown in Figure 1(a). The unit cell of the structure consists of a metallic patch imprinted on the top surface of a FR4 dielectric substrate ($\varepsilon_r = 4.25$ and $\tan\,\delta = 0.02$) having 1 mm thickness whose bottom side is completely metal laminated. Both the top metallic patch and ground plane are made of copper ($\sigma = 5.8 \times 10^7$ S/m) of thickness 0.035 mm. The geometrical dimensions of the structure are also mentioned in Figure 1(a).

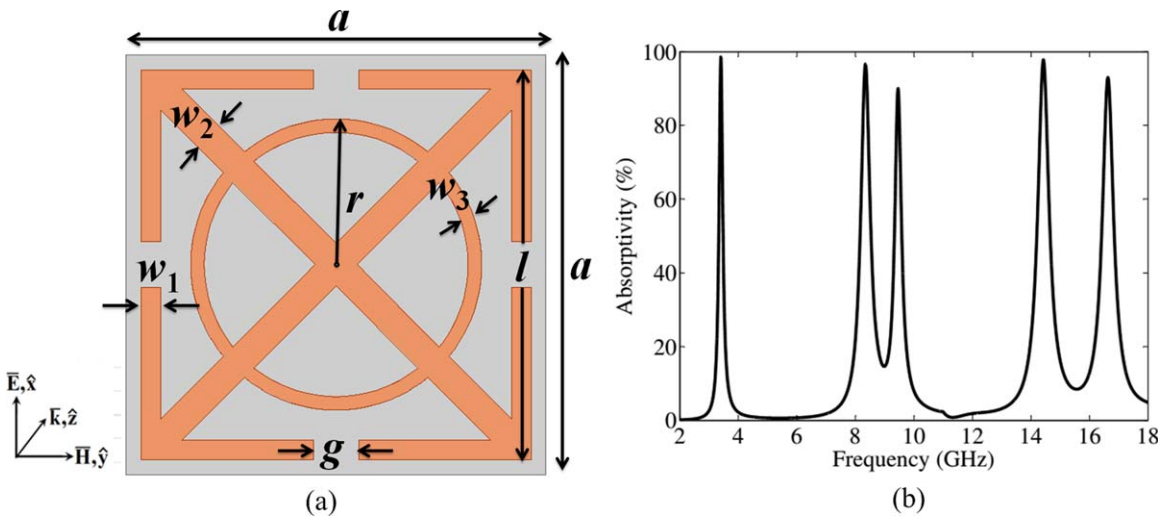

Figure 1 (a) Top view of the unit cell of the proposed penta-band structure with geometrical dimensions: $a = 14$, $l = 13$, $g = 1.5$, $w_1 = 1.3$, $w_2 = 1$, $w_3 = 0.45$, $r = 4.85$ (unit: mm) with and (b) simulated absorptivity responses. [Color figure can be viewed in the online issue, which is available at wileyonlinelibrary.com]

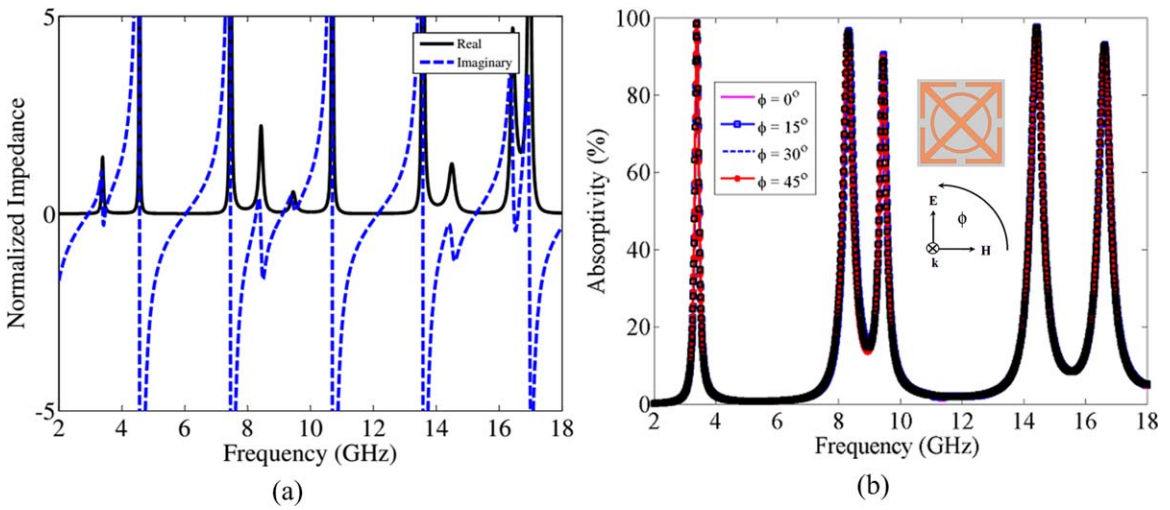

Figure 2 (a) Retrieved normalized input impedance and (b) simulated absorptivity response for different polarization angles under normal incidence of the proposed structure. [Color figure can be viewed in the online issue, which is available at wileyonlinelibrary.com]

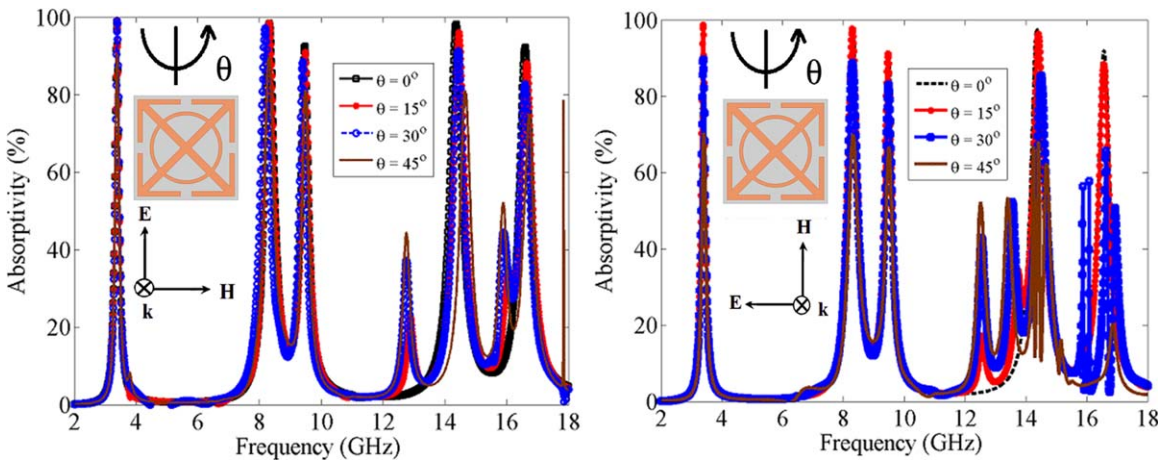

Figure 3 Simulated absorptivity responses under oblique incidence condition for (a) TE and (b) TM polarizations. [Color figure can be viewed in the online issue, which is available at wileyonlinelibrary.com]

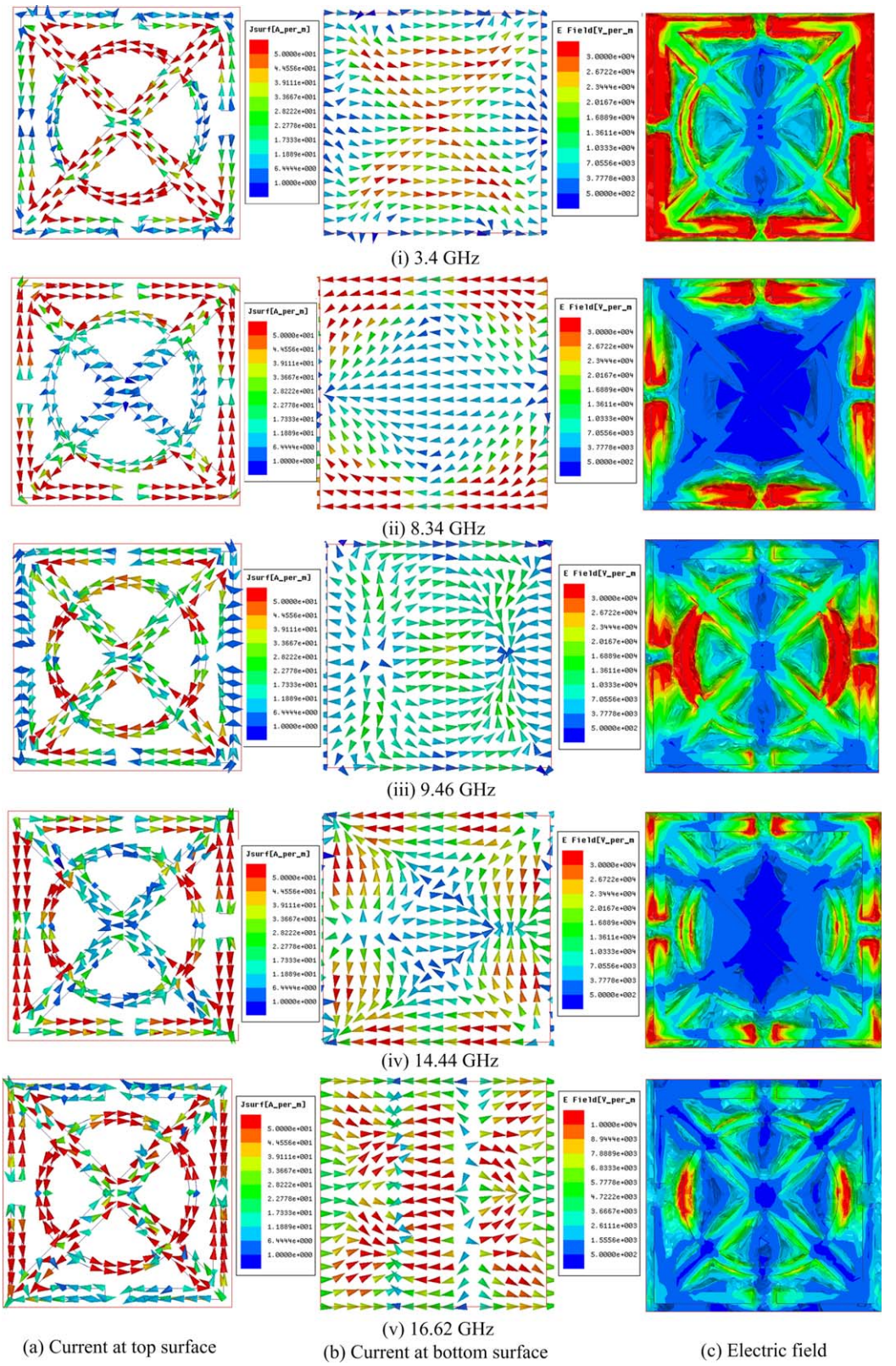

Figure 4 (a) Current distribution on top surface, (b) current distribution on bottom surface, and (c) electric field distribution of the proposed structure at peak absorption frequencies. [Color figure can be viewed in the online issue, which is available at wileyonlinelibrary.com]

Absorptivity $A(\omega)$ of the structure can be determined from (1), where $A(\omega)$, $|S_{11}(\omega)|^2$, $|S_{21}(\omega)|^2$ denote absorptivity, reflected power, and transmitted power, respectively

$$A(\omega) = 1 - |S_{11}(\omega)|^2 - |S_{21}(\omega)|^2. \quad (1)$$

Due to complete copper backing, no transmission ($|S_{21}(\omega)| = 0$) of incident electromagnetic wave (EM) takes place

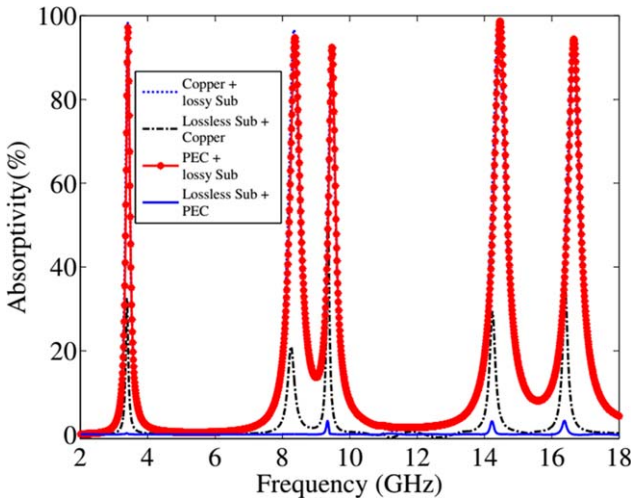

Figure 5 Comparison of absorptivities under different losses of the structure. [Color figure can be viewed in the online issue, which is available at wileyonlinelibrary.com]

and the absorptivity can be calculated solely from the reflected power. Henceforth, we can conclude that $A(\omega)$ can be maximized by minimizing the reflection from the structure.

The proposed absorber has been simulated in finite element method based Ansys HFSS where periodic boundary conditions have been applied along "x" and "y" axis. The structure exhibits five distinct absorption peaks at 3.4, 8.34, 9.46, 14.44, and 16.62 GHz with peak absorptivities of 98.6%, 96.6%, 90.1%, 97.8%, and 93.1%, respectively, as shown in Figure 1(b).

It can also be concluded that by optimizing the physical parameters of the top copper surface and thickness of the dielectric substrate, both the electric and magnetic responses can be tuned in such a way so that the input impedance of the structure $Z(\omega)$ is perfectly matched with free space impedance η_0 at a particular frequency. At that frequency, reflection coefficient $|S_{11}(\omega)|$ gets minimized as evident from (2) and near-unity absorptivity can be realized

$$S_{11}(\omega) = \frac{Z(\omega) - \eta_0}{Z(\omega) + \eta_0}. \tag{2}$$

The normalized input impedance result is shown in Figure 2(a). The real and imaginary parts of the normalized input impedance are close to unity and infinite, respectively, at these five distinct frequency bands [19].

The proposed structure has been studied for different polarization angles. Due to the fourfold symmetrical design, the structure has been studied up to 45° polarization angles as shown in Figure 2(b) and it is clear that the structure is polarization-insensitive in nature under normal incident angles. The structure has been studied under oblique incidences for both TE and TM polarizations. In TE polarization the electric field direction is kept constant while the magnetic field and the wave vector directions have been changed to realize oblique incidence. In TM polarization the magnetic field direction is kept constant while electric field along with wave vector directions has been changed up to 45°. The simulated absorptivity responses for these cases are shown in Figures 3(a) and 3(b), respectively, where five distinct absorption peaks have been illustrated. It is observed that high absorption (∼80%) up to 45° of incident angles, has been achieved under oblique incidence. The additional peaks, in particular at higher frequencies, have been observed at higher incident angles for both TE and TM polarizations as shown in Figure 3 which may be due to higher order resonant modes.

Surface current density distributions on the top and bottom surfaces at different absorption frequencies have been illustrated in Figure 4. At 3.4 GHz, the inner ring along with cross part is mainly responsible for localizing the surface current whereas most of the surface currents have been distributed within outer split square ring at 8.34 GHz as shown in Figures 4(i) and [4](ii), respectively. Surface current distributions for other three frequencies at 9.46, 14.44, and 16.62 GHz have been shown in Figures 4(iii), [4](iv), and [4](v), respectively.

From Figure 4, it can also be noted that the surface current distributions on top and bottom copper surface are in antiparallel direction for all five distinct absorption peaks. These two opposite surface currents constitute a circulating current loop and it is in perpendicular plane to the direction of the incident magnetic field [20]. On the contrary as the top metallic patch is excited by the incident electric field as shown in Figure 4(c), the electric resonance can be controlled by tuning the geometrical dimensions of the structure. Thus, strong electromagnetic absorptions take place at these five distinct frequency bands.

In Figure 5, the origin of different losses of the structure has been investigated by tuning different material properties. When

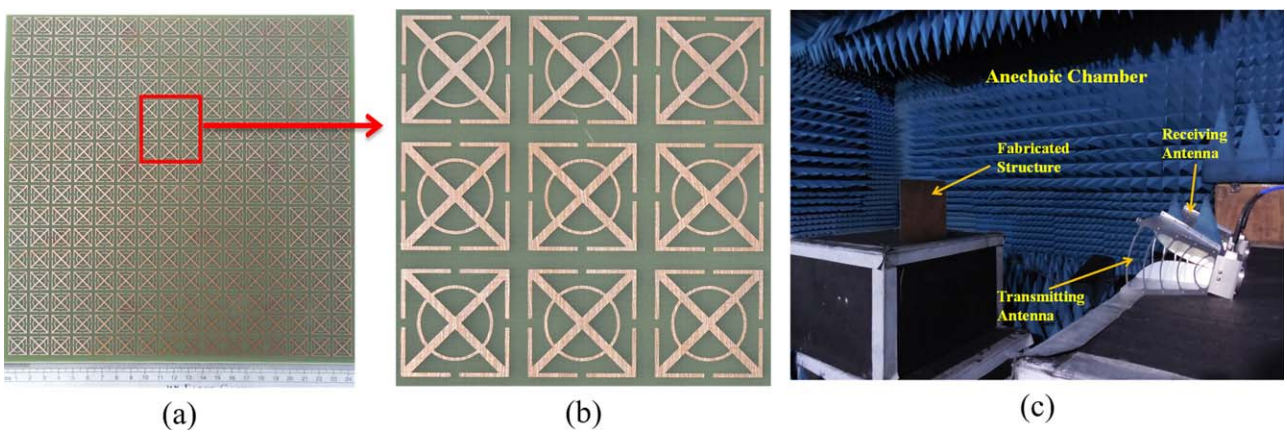

Figure 6 (a) Fabricated penta-band structure, with (b) enlarged view, and (c) experimental arrangement within the anechoic chamber. [Color figure can be viewed in the online issue, which is available at wileyonlinelibrary.com]

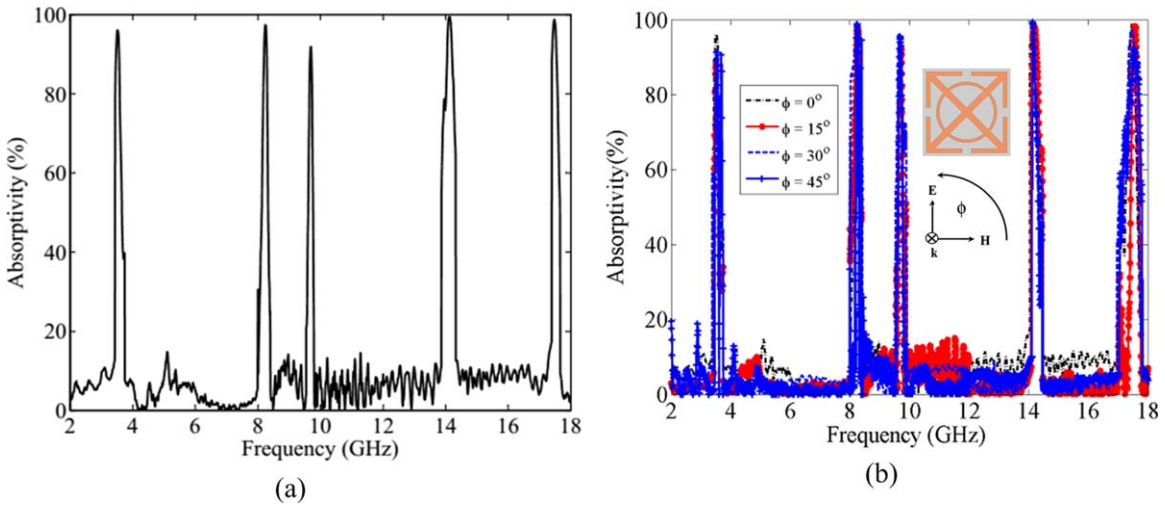

Figure 7 (a) Measured absorptivity plot and (b) measured absorptivity response for different polarization angles under normal incidence of the penta-band structure. [Color figure can be viewed in the online issue, which is available at wileyonlinelibrary.com]

the copper sheet is replaced by the perfect electric conductor, the absorption peaks decrease very slightly validating the small contribution of ohmic loss in absorption. When the dielectric loss tangent has been changed from 0.025 to 0, the absorptivities for five distinct peaks decrease drastically. Hence, it clearly depicts that the dielectric loss is mainly responsible for the absorption mechanism of the structure. When both the ohmic loss and dielectric loss are absent in the structure, the total absorptivities for the five distinct peaks is reduced to zero as shown by blue line in Figure 5.

3. EXPERIMENTAL RESULTS

The proposed structure has been fabricated with dimensions of 256 × 256 mm^2 on a planar sheet of 1 mm thick FR4 substrate using standard printed circuit board technology. The complete fabricated structure has been shown in Figure 6(a) along with enlarged view in Figure 6(b).

A pair of standard broadband horn antennas (LB-10180-SF operating in 1–18 GHz) which are connected to an Agilent N5230A vector network analyzer has been used for measuring the reflectivity of the proposed structure where one antenna has been used as transmitting EM wave and another one is for receiving the same. Initially, an identical copper plate is placed in the anechoic chamber and the reflection from its surface has been measured. Then, the copper plate is replaced by the fabricated structure and reflection from its surface has been measured. Now the actual reflection from the structure has been calculated by subtracting the reflected power from the structure than that of the copper surface. From this the absorptivity has been calculated. The experimental setup for measurement is shown in Figure 6(c).

The measured absorptivity plot is shown in Figure 7(a). The measured results show that the absorptivities occur at frequencies 3.52, 8.24, 9.69, 14.12, and 17.48 GHz with peak absorptivity values of 96.1%, 97.4%, 91.9%, 99.5%, and 98.8%, respectively. It can be noted that the small deviation of measured responses from the simulation results may be due to fabrication tolerance.

The reflectivity of the structure has been measured for different polarization angles under normal incidence by rotating the

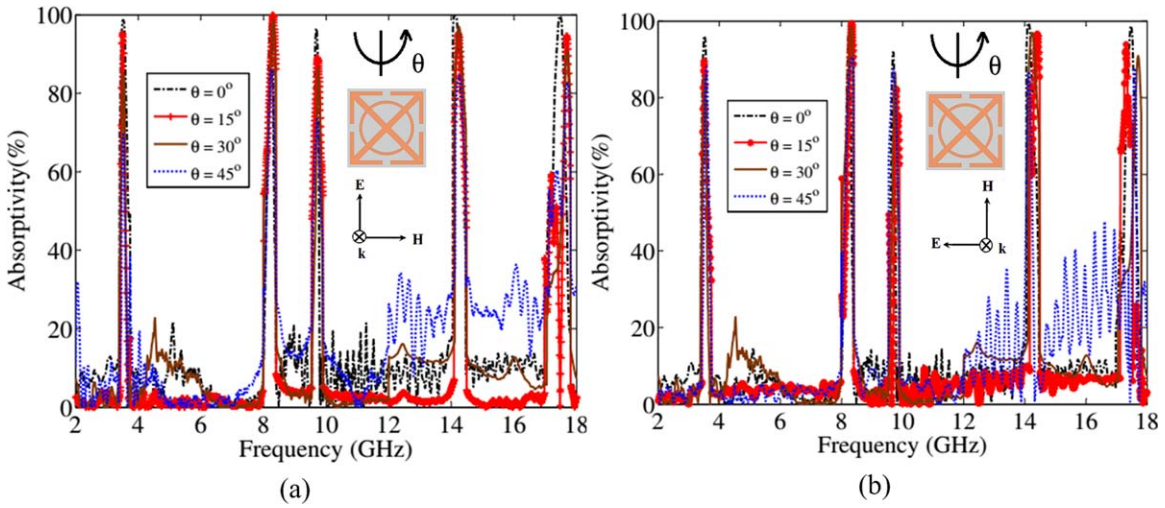

Figure 8 Measured absorptivity under oblique incidence condition for (a) TE and (b) TM polarizations. [Color figure can be viewed in the online issue, which is available at wileyonlinelibrary.com]

TABLE 1 Comparison among Multiband Absorbers

Parameter	Unit Cell Size (mm)	Unit Cell Size Corresponding to Lowest Frequency	Thickness (mm)	Thickness Corresponding to Lowest Frequency
Ref. 13	23	$0.3\lambda_0$	1	$0.013\lambda_0$
Ref. 14	20	$0.169\lambda_0$	1.5	$0.012\lambda_0$
Ref. 15	10	$0.223\lambda_0$	1	$0.022\lambda_0$
Proposed structure	14	$0.159\lambda_0$	1	$0.011\lambda_0$

structure around its axis, keeping the two antennas at fixed position. The measured response for different polarization angles under normal incidence has been shown in Figure 7(b). It is clear from the measured response that the structure is polarization-insensitive exhibiting five distinct frequency bands. Figures 8(a) and 8(b) show the measured absorptivities for TE and TM polarizations, respectively, under oblique incident angle ranging from 0° to 45°. For both the polarizations, the structure exhibits high absorption peaks up to 45° oblique incidence with additional peaks occurring at higher frequencies as observed from Figure 8.

4. CONCLUSION

A tetra-arrow resonator integrated with an inner circular ring structure has been proposed as a penta-band MTM absorber. The geometrical dimensions of the proposed structure have been optimized in such a way so that it provides five distinct absorption peaks at the International Telecommunications Union specified bands designated for airborne radar systems [21]. The proposed absorber is much more compact and ultrathin as compared with the previously reported multiband absorbers in the literature and the comparison among those absorbers in terms of the unit cell dimension and thickness has been enlisted in Table 1. The proposed MTM absorber has the advantages of miniaturization and structural symmetry in design. To better visualize the absorption mechanism of the proposed absorber, surface current distributions, and electric field distributions at the five distinct frequencies of absorption have been plotted. In addition, the proposed absorber has been fabricated and experimental results are in good agreement with the simulated responses. The measured responses affirm that the structure is polarization-insensitive under normal incidence. It also shows good absorption over a wide angle of incidence for both theoretical as well as experimental studies. Hence, the proposed absorber can be a good candidate for various potential applications like airborne radar, stealth technology, and radome applications.

ACKNOWLEDGMENT

This work is partially supported by ISRO, SAC under Project No. SPO/STC/EE/2014087.

REFERENCES

1. D.R. Smith, W.J. Padilla, D.C. Vier, S.C. Nemat-Nasser, and S. Schultz, Composite medium with simultaneously negative permeability and permittivity, Phys Rev Lett 84 (2000), 4184–4187.
2. N.I. Landy, S. Sajuyigbe, J.J. Mock, D.R. Smith, and W.J. Padilla, Perfect metamaterial absorber, Phys Rev Lett 100 (2008), 207402
3. N. Fang, H. Lee, C. Sun, and X. Zhang, Sub-diffraction-limited optical imaging with a silver superlens, Science 308 (2005), 534–537.
4. S.A. Cummer, B.I. Popa, D. Schurig, D.R. Smith, and J.B. Pendry, Full wave simulations of electromagnetic cloaking structures, Phys Rev E 74 (2006), 036621
5. K. Alici and E. Ozbay, Radiation properties of a split ring resonator and monopole composite, Phys Stat Sol (b) 244 (2007), 1192–1196.
6. C. Caloz and T. Itoh, Electromagnetic metamaterials: Transmission line theory and microwave applications, Wiley-IEEE Press, 2005.
7. F. Capolino, Metamaterials handbook, CRC Press, 2009.
8. F. Bilotti, L. Nucci, and L. Vegni, An SRR-based microwave absorber, Microwave Opt Technol Lett 48 (2006), 2171–2175.
9. B. Ni, X.S. Chen, L.J. Huang, J.Y. Ding, G.H. Li, and W. Lu, A dual-band polarization insensitive metamaterial absorber with split ring resonator, Opt Quantum Elect 45 (2013), 747–753.
10. H.M. Lee and H.S. Lee, A dual band metamaterial absorber based with resonant-magnetic structures, Prog Electromag Res 33 (2012), 1–12.
11. S. Bhattacharyya, S. Ghosh, and K.V. Srivastava, Triple band polarization-independent metamaterial absorber with bandwidth enhancement at X-band, J Appl Phys 114 (2013), 094514
12. S. Bhattacharyya and K.V. Srivastava, Triple band polarization-independent ultra-thin metamaterial absorber using ELC resonator, J Appl Phys 15 (2014), 064508
13. D. Chaurasiya, S. Ghosh, S. Bhattacharyya, and K.V. Srivastava, An ultra-thin quad-band polarization-insensitive wide-angle metamaterial absorber, Microwave Opt Techol Lett 57 (2015), 697–702.
14. Z. Mao, S. Liu, B. Bian, B. Wang, B. Ma, L. Chen, and J. Xu, Multi-band polarization-insensitive metamaterial absorber based on Chinese ancient coin-shaped structures, J Appl Phys 115 (2014), 204505
15. W. Wang, M. Yan, Y. Pang, J. Wang, H. Ma, S. Qua, H. Chen, C. Xu, and M. Feng, Ultra-thin quadri-band metamaterial absorber based on spiral structure, Appl Phys A 118 (2015), 443–447.
16. S. Ghosh, S. Bhattacharyya, and K.V. Srivastava, Bandwidth-enhancement of an ultra-thin polarization insensitive metamaterial absorber, Microwave Opt Technol Lett 56 (2014), 350–355.
17. S. Ghosh, S. Bhattacharyya, and K.V. Srivastava, Bandwidth-enhanced polarization-insensitive microwave metamaterial absorber and its equivalent circuit model, J Appl Phys 115 (2014), 104503
18. J. Lee and S. Lim, Bandwidth-enhanced and polarization-insensitive metamaterial absorber using double resonance, Electron Lett 47 (2011), 8–9.
19. F. Costa, S. Genovesi, and A. Monorchio, On the bandwidth of high-impedance frequency selective surfaces, IEEE Antennas Wireless Propag Lett 8 (2009), 1341–1344.
20. M. Kafesaki, I. Tsiapa, N. Katsarakis, T. Koschny, C.M. Soukoulis, and E.N. Economou, Left-handed metamaterials: The fishnet structure and its variations, Phy Rev B 75 (2007), 235114
21. Available at: http://copradar.com/preview/chapt7/ch7d1.html.

CMOS LOW NOISE AMPLIFIER DESIGNS FOR 5.8 GHz DEDICATED SHORT-RANGE COMMUNICATIONS APPLICATIONS

Chien-Chang Huang and George Changlin Guu
Department of Communication Engineering, Yuan Ze University, 135, Yuan-Tung Road, Chung-Li, Taoyuan, 32003, Taiwan;
Corresponding author: cch@saturn.yzu.edu.tw

Received 4 April 2015

ABSTRACT: *This article presents two low noise amplifier (LNA) designs in 5.8 GHz using 0.18 μm CMOS technology, for dedicated short-range communications (DSRC) applications. The source degenerate inductor is utilized for the cascode configuration with and without the mutual coupling from the gate inductor, to show the compromise*